Simulation Analysis of Quasi Space Vector PWM in Different Conduction Modes for Inverter Fed Permanent Magnet Brushless DC Motor Drive

Yossawee Weerakamhaeng*
Department of Electrical and Computer Engineering, Faculty of Engineering,
Thammasat University, Rangsit Campus,
Khlong Nueng, Khlong Luang, Pathum Thani, 12120 Thailand

Abstract

It is known that the Space Vector PWM (SVPWM) modulation scheme is superior in driving a three-phase permanent magnet brushless dc (3PPMBLDC) motor through the use of conventional three-phase voltage source inverter (3PVSI). However, implementing SVPWM in an embedded system requires that a high performance chip, such as a DSP chip, be used, not economically suitable for low precision applications such as electric bike motor drive and quad rotor robot motor drive. For these applications, it is acceptable to adopt a 3PVSI with a simpler modulation scheme that can be classified into 3 types, namely, the 120° conduction mode quasi SVPWM (120° QSVPWM), the 150° conduction mode quasi SVPWM (150° QSVPWM), and the 180° conduction mode quasi SVPWM (180° QSVPWM). This paper describes all three modulation schemes and conducts a performance analysis of the 3PVSIs resulting from applying each of the modulation schemes. The performance numbers are obtained through simulations. Eventually, our custom built simulated dynamic model of 3PPMBLDC motor based on the Simulink package in MATLAB software is brought to be verified by our custom built simulated model of 3PVSI with different modulation schemes in order to visualize the torque and mechanical angular velocity(speed) characteristics.

Keywords: Voltage source inverter conduction mode; three phase brushless DC motor drive; space vector voltage source inverter.

***Correspondence :** wyossawe@engr.tu.ac.th

Nomenclature

θ_e	Electrical angular displacement.
V_{a0}	Voltage at point a with respect to point 0.
θ_m	Mechanical angular displacement.
$\overrightarrow{v}_s^{\alpha\beta}$	Voltage space vector with respect to the $\alpha-\beta$ reference frame.
$S_1,\ldots,S_6$	Switching elements $1,\ldots,6$
d	The normalized duty cycle.
$e_m(t)$	The peak value of back EMF.
K_b	The motor back EMF constant (volt/(rad/s)).
$e_a(t,\theta_e)$	The back EMF of the stator windings, phase a
$\omega_m(t)$	The mechanical angular velocity of the rotor.
T_e	The electromagnetic torque.
J_m	The moment of inertia of the rotor including mechanical loads attached.
B_m	The viscous damping between the rotor and the environment contacted.
T_l	The load torque disturbed through the axle of rotor.
$\omega_e(t)$	The rotor electrical angular velocity.
p	The number of poles of permanent magnets attached to the rotor.
M	The mutual inductance between each phase winding
L	The self inductance of each phase winding.
R_p	The resistance of each phase winding.
$L_p = L - M$	The self against mutual inductance difference.

1. Introduction

It is beneficial to use SVPWM as the modulation scheme for the operation of a 3PVSI when driving a 3PPMBLDC motor. However, most studies in the literature cover only the so-called "120° conduction mode" and "180° conduction mode" [3,6,7,8,9,10]. which are the modes of which, when applied by 100% duty cycle gating signal to each switching element, the conduction duration allowable to each switching element to conduct for 120° or 180° electrical angular displacement(θ_e) respectively, in each switching cycle. Considering the possible combinations of all six switches in the power stage of 3PVSI, it is possible to have one more mode called the 150° conduction mode, a mode that has been mentioned in the literature [1]. In [1], 3PVSI was used to drive the three phase induction motor. However, the study did not cover the use of a 3PPMBLDC motor. No existing work, to the best of our knowledge, demonstrates what happens when one drives a 3PPMBLDC motor using a 3PVSI in this mode. This study then reveals the behaviors of a 3PVSI while carrying out all of three aforementioned

conduction modes in driving a 3PPMBLDC motor. The torque and mechanical angular velocity (speed) of this motor are examined as well through simulation results. The models of a 3PVSI and a 3PPMBLDC motor are created to explore various aspects of interest. The creation of the models is based on Simulink, packages in MATLAB software. Since SVPWM is computationally intensive, implementing it in an embedded system requires that a high performance processor, such as a DSP chip, be used. This requirement drives up the cost and makes it difficult to employ SVPWM in low precision applications such as electric bike motor drive and quad rotor robot motor drive. In order to accommodate applications with lower precision and computation requirements, this study proposes the concept of the quasi space vector (QSV) upon which three aforementioned modulation schemes are based. QSV is a space vector rotating stepwise at a fixed electrical angular displacement (θ_e) whereas a space vector (SV) may rotate continuously in the reference coordinate system.

2. Conventional 3PVSI driving 3PPMBLDC motor

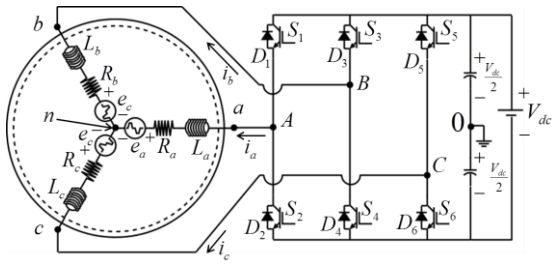

Fig.1. The power stage of a three-phase VSI fed 3PPMBLDC Motor Drive.

From Fig. 1, $S_1,\ldots,S_6$ are the switching elements (such as MOSFETs or IGBTs) that can have the states of "on" or "off" with the constraint of the shoot-through prohibited condition. The voltage at points a,b,c with respect to point 0 denoted (V_{a0},V_{b0},V_{c0}), can have three possible values, namely, $V_{dc}/2$, $-V_{dc}/2$, and the value between these two voltage levels. With the load balanced condition of $V_{an}+V_{bn}+V_{cn}=0$, it can be shown that

$$V_{n0}=\frac{1}{3}[V_{a0}+V_{b0}+V_{c0}], \quad (1)$$

$$V_{an}=V_{a0}-V_{n0}, \quad (2)$$

$$V_{bn}=V_{b0}-V_{n0}, \quad (3)$$

$$V_{cn}=V_{c0}-V_{n0} \quad (4)$$

2.1 Space Vector and Quasi Space Vector Definitions

A space vector (SV) is a rotating vector representing three sinusoidal phase quantities in the same system. It can be rotated continuously in space. This study considers the voltage space vector, $\vec{v}_s$, of the three balanced sinusoidal phase voltages, comprising $v_{an}=v_m\cos(\omega_e t)$, $v_{bn}=v_m\cos(\omega_e t-2\pi/3)$ and $v_{cn}=v_m\cos(\omega_e t+2\pi/3)$ where ω_e is the electrical angular velocity. We define the two dimensional reference frame, called the $\alpha-\beta$ reference frame, as the fixed frame. The voltage space vector with respect to this frame can be written as $\vec{v}_s^{\,\alpha\beta}$ and can be calculated as in Eq. (5) (phase invariant form) :

$$\vec{v}_s^{\,\alpha\beta}=\frac{2}{3}\left(\vec{v}_{an}^{\,\alpha\beta}+\vec{v}_{bn}^{\,\alpha\beta}+\vec{v}_{cn}^{\,\alpha\beta}\right). \quad (5)$$

A depiction of $\vec{v}_s^{\,\alpha\beta}$ is shown in Fig. 2.

Quasi Space Vector (QSV) Definition. QSV is a space vector rotating stepwise by a fixed electrical angular displacement(θ_e).

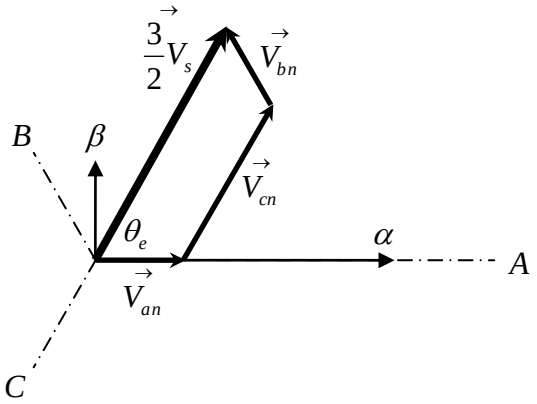

Fig.2. The voltage space vector denoted $\vec{v}_s^{\alpha\beta}$, as the vector summation of three sinusoidal phase voltage vectors, $\vec{v}_{an}^{\alpha\beta}, \vec{v}_{bn}^{\alpha\beta}, \vec{v}_{cn}^{\alpha\beta}$

2.2 3PVSI in 120°, 150°, and 180° conduction mode square wave outputs

2.2.1 3PVSI in 120° conduction mode

In this mode, the conduction duration allowed for each switching element ($S_1,\ldots,S_6$) of a 3PVSI as shown in Fig. 1 is equal to 120° of θ_e in each switching cycle. The voltages, $V_{A0}, V_{B0}, V_{C0}, V_{n0}, V_{an}, V_{bn}$ and V_{cn} for a 3PVSI with the 120° conduction mode applied by 100% duty cycle gating signal to each switching element can be depicted in Fig. 4 . It is clear that there are 3 possible levels of voltages, V_{an}, V_{bn}, and V_{cn}, each of which is $V_{dc}/2$, 0, $-V_{dc}/2$ consecutively. From Eq. (5), $\vec{v}_s^{\alpha\beta}$ can be displayed in the diagram of Fig. 3. From this diagram, $\vec{v}_s^{\alpha\beta}$ rotates discontinuously at the step size of $\pi/3$ radians such as from $\vec{V}_{61}$ to $\vec{V}_{12}$. $\vec{v}_s^{\alpha\beta}$ in this mode is the QSV. The Fourier series representing V_{an} with the period of 2π can be written as:

$$V_{an}(\theta_e) = \sum_{m=1}^{\infty}\left(V_{dc}/m\pi\right)\left(\sin\left(\frac{m\pi}{3}\right)\right)^2 \bullet$$

$$\left[1-2\cos(\frac{m\pi}{3})-2\cos(m\pi)\right]\sin(m\theta_e). \qquad (6)$$

The fundamental component of V_{an}, $HV_{an}\big|_{m=1}$, is equal to $3V_{dc}/2\pi$.

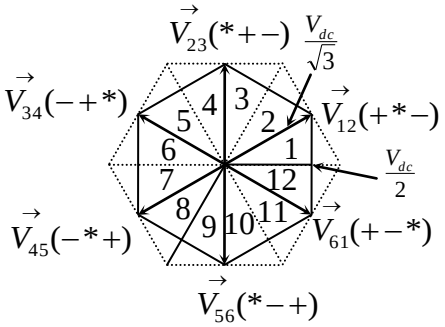

Fig.3. Diagram depicting the 120° conduction mode voltage space vector, $\vec{v}_s^{\alpha\beta}$.

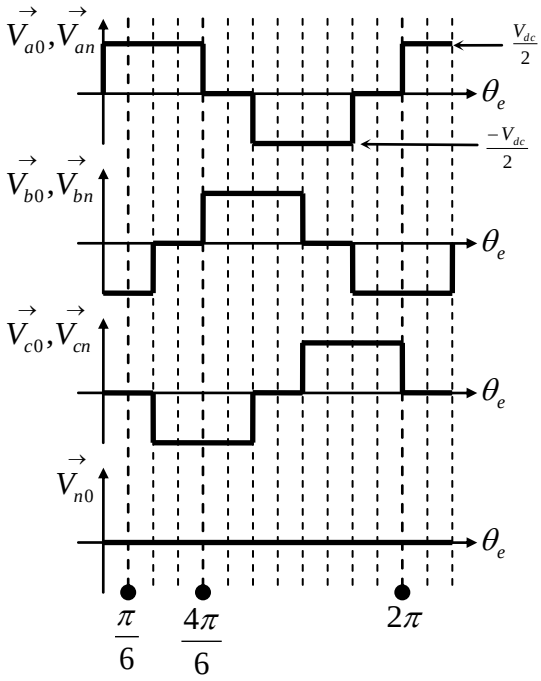

Fig.4. The voltages, $V_{A0},V_{B0},V_{C0},V_{n0},V_{an},V_{bn},$ and V_{cn} for a 3PVSI in the 120° conduction mode applied by 100% duty cycle gating signals.

3PVSI in 150° conduction mode

In this mode, the conduction duration allowed for each switching element ($S_1,\ldots,S_6$) of a 3PVSI as shown in Fig. 1 is equal to 150° of θ_e in each switching cycle. The voltages, $V_{A0},V_{B0},V_{C0},V_{n0},V_{an},V_{bn}$ and V_{cn} for a 3PVSI with the 150° conduction mode applied by 100% duty cycle gating signal to each switching element can be depicted in Fig. 7. It is clear that there are 7 possible levels of voltages for $V_{an},V_{bn},$ and $V_{cn},$ each of which is $0, \pm V_{dc}/3, \pm V_{dc}/2, \pm 2V_{dc}/3$, consecutively.

From Eq. (5), $\vec{v}_s^{\,\alpha\beta}$ can be displayed in the diagram of Fig. 5. From this diagram, $\vec{v}_s^{\,\alpha\beta}$ rotates discontinuously at the step size of $\pi/6$ radians such as from $\vec{V}_{61}$ to $\vec{V}_1$. $\vec{v}_s^{\,\alpha\beta}$ in this mode is the QSV. The Fourier series representing V_{an} with the period of 2π can be written as:

$$V_{an}(\theta_e)=\sum_{m=1}^{\infty}\frac{2V_{dc}}{3m\pi}\left(\sin(\frac{m\pi}{6})\right)^2 \bullet \left[\left(3-6\cos(\frac{m\pi}{6})+4\cos(\frac{m\pi}{3})\right.\right.$$
$$-7\cos(\frac{m\pi}{2})+\cos(\frac{2m\pi}{3})-7\cos(\frac{5m\pi}{6})$$
$$-\cos(m\pi)-5\cos(\frac{7m\pi}{6})-\cos(\frac{4m\pi}{3})$$
$$\left.-2\cos(\frac{3m\pi}{2})\right]\sin(m\theta_e). \qquad (7)$$

The fundamental component of V_{an}, $HV_{an}\big|_{m=1}$ is equal to $(2+\sqrt{3})V_{dc}/2\pi$.

3PVSI in 180° conduction mode

In this mode, the conduction duration allowed for each switching element ($S_1,\ldots,S_6$) of a 3PVSI as shown in Fig. 1 is equal to 180° of θ_e in each switching cycle. The voltages, $V_{A0},V_{B0},V_{C0},V_{n0},V_{an},V_{bn}$ and V_{cn} for a 3PVSI with the 180° conduction mode applied by 100% duty cycle gating signal to each switching element can be depicted as in Fig. 8 . It is clear that there are 3 possible levels of voltages for $V_{an},V_{bn},$ and $V_{cn},$ each of which is $V_{dc}/2, 0, -V_{dc}/2$ consecutively. From Eq. (5), $\vec{v}_s^{\,\alpha\beta}$ can be displayed in the diagram of Fig.6. From this diagram, $\vec{v}_s^{\,\alpha\beta}$ rotates discontinuously at the step size of $\pi/3$ radians

such as from $\vec{V}_1$ to $\vec{V}_2$. $\vec{v}_s^{\alpha\beta}$ in this mode is the QSV. The Fourier series representing V_{an} with the period of 2π can be written as:

$$V_{an}(\theta_e)=\sum_{m=1}^{\infty}\frac{4V_{dc}}{3m\pi}\left(\sin(\frac{m\pi}{3})\right)^2 \bullet$$

$$\left[-\cos(\frac{2m\pi}{3})-\cos(m\pi)-\cos(\frac{4m\pi}{3})\right]\sin(m\theta_e). \qquad (8)$$

The fundamental component of V_{an}, $HV_{an}\big|_{m=1}$ is equal to $2V_{dc}/\pi$.

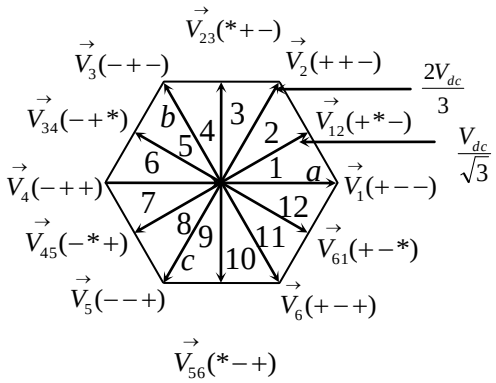

Fig.5. Diagram depicting the 150° conduction mode voltage space vector, $\vec{v}_s^{\alpha\beta}$.

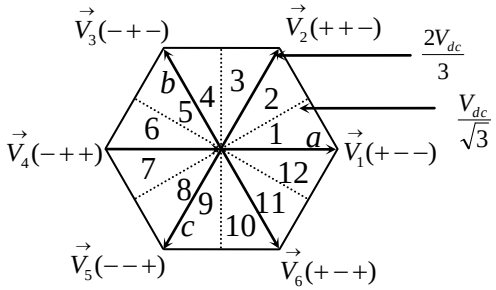

Fig.6. Diagram depicting the 180° conduction mode voltage space vector, $\vec{v}_s^{\alpha\beta}$.

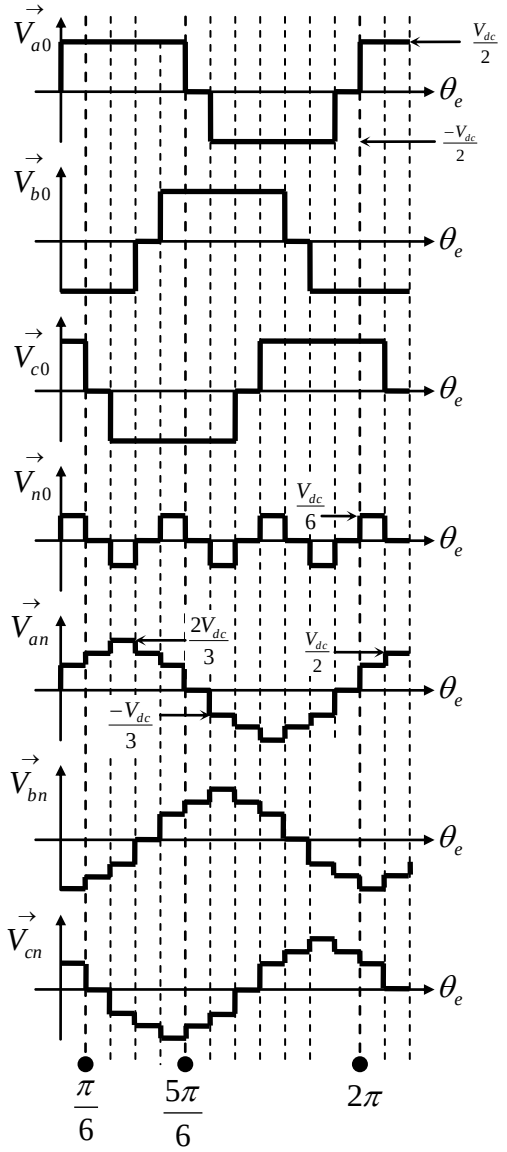

Fig.7. The voltages, $V_{A0},V_{B0},V_{C0},V_{n0},V_{an},V_{bn},V_{cn}$ for 3PVSI with the 150° conduction mode applied by 100% duty cycle gating signals.

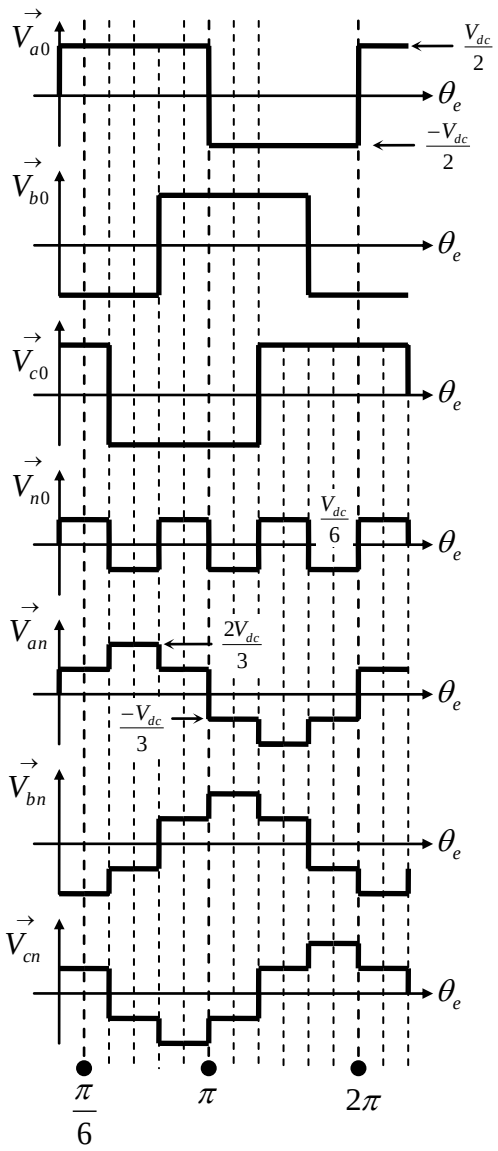

Fig.8. The voltages, $V_{A0},V_{B0},V_{C0},V_{n0},V_{an},V_{bn},V_{cn}$ for 3PVSI with the 180° conduction mode applied by 100% duty cycle gating signals.

The switching patterns, $V_{A0},V_{B0},V_{C0},V_{n0}$,$V_{an},V_{bn},$ and V_{cn} can be tabulated as shown in Table. 1

Table 1. Relationships between QSVs and switching patterns.

$\vec{v}_s$	Voltage states	**"on"** switches	$V_{A0},V_{B0},V_{C0},V_{n0}$	V_{an},V_{bn},V_{cn}
$\vec{v}_{Z1}$	(−−−)	$S_2S_4S_6$	$\frac{-V_{dc}}{2},\frac{-V_{dc}}{2},\frac{-V_{dc}}{2},\frac{-V_{dc}}{2}$	0,0,0
$\vec{v}_{Z2}$	(−−*)	S_2S_4	$\frac{-V_{dc}}{2},\frac{-V_{dc}}{2},\frac{-V_{dc}}{2},\frac{-V_{dc}}{2}$	0,0,0
$\vec{v}_5$	(−−+)	$S_2S_4S_5$	$\frac{-V_{dc}}{2},\frac{-V_{dc}}{2},\frac{V_{dc}}{2},\frac{-V_{dc}}{6}$	$\frac{-V_{dc}}{3},\frac{-V_{dc}}{3},\frac{2V_{dc}}{3}$
$\vec{v}_{Z3}$	(−*−)	S_2S_6	$\frac{-V_{dc}}{2},\frac{-V_{dc}}{2},\frac{-V_{dc}}{2},\frac{-V_{dc}}{2}$	0,0,0
$\vec{v}_{Z4}$	(−**)	S_2	$\frac{-V_{dc}}{2},\frac{-V_{dc}}{2},\frac{-V_{dc}}{2},\frac{-V_{dc}}{2}$	0,0,0
$\vec{v}_{4,5}$	(−*+)	S_2S_5	$\frac{-V_{dc}}{2},0,\frac{V_{dc}}{2},0$	$\frac{-V_{dc}}{2},0,\frac{V_{dc}}{2}$
$\vec{v}_3$	(−+−)	$S_2S_3S_6$	$\frac{-V_{dc}}{2},\frac{V_{dc}}{2},\frac{-V_{dc}}{2},\frac{-V_{dc}}{6}$	$\frac{-V_{dc}}{3},\frac{2V_{dc}}{3},\frac{-V_{dc}}{3}$
$\vec{v}_{3,4}$	(−+*)	S_2S_3	$\frac{-V_{dc}}{2},\frac{V_{dc}}{2},0,0$	$\frac{-V_{dc}}{2},\frac{V_{dc}}{2},0$
$\vec{v}_4$	(−++)	$S_2S_3S_5$	$\frac{-V_{dc}}{2},\frac{V_{dc}}{2},\frac{V_{dc}}{2},\frac{V_{dc}}{6}$	$\frac{-2V_{dc}}{3},\frac{V_{dc}}{3},\frac{V_{dc}}{3}$
$\vec{v}_{Z5}$	(*−−)	S_4S_6	$\frac{-V_{dc}}{2},\frac{-V_{dc}}{2},\frac{-V_{dc}}{2},\frac{-V_{dc}}{2}$	0,0,0
$\vec{v}_{Z6}$	(*−*)	S_4	$\frac{-V_{dc}}{2},\frac{-V_{dc}}{2},\frac{-V_{dc}}{2},\frac{-V_{dc}}{2}$	0,0,0
$\vec{v}_{5,6}$	(*−+)	S_4S_5	$0,\frac{-V_{dc}}{2},\frac{V_{dc}}{2},0$	$0,\frac{-V_{dc}}{2},\frac{V_{dc}}{2}$
$\vec{v}_{Z7}$	(**−)	S_6	$\frac{-V_{dc}}{2},\frac{-V_{dc}}{2},\frac{-V_{dc}}{2},\frac{-V_{dc}}{2}$	0,0,0
$\vec{v}_{Z8}$	(***)		$V_{a0},V_{a0},V_{a0},V_{a0}$	0,0,0
$\vec{v}_{Z9}$	(**+)	S_5	$\frac{V_{dc}}{2},\frac{V_{dc}}{2},\frac{V_{dc}}{2},\frac{V_{dc}}{2}$	0,0,0
$\vec{v}_{2,3}$	(*+−)	S_3S_6	$0,\frac{V_{dc}}{2},\frac{-V_{dc}}{2},0$	$0,\frac{V_{dc}}{2},\frac{-V_{dc}}{2}$
$\vec{v}_{Z10}$	(*+*)	S_3	$\frac{V_{dc}}{2},\frac{V_{dc}}{2},\frac{V_{dc}}{2},\frac{V_{dc}}{2}$	0,0,0

$\vec{v}_{Z11}$	(*++)	S_3S_5	$\frac{V_{dc}}{2},\frac{V_{dc}}{2},\frac{V_{dc}}{2},\frac{V_{dc}}{2}$	0,0,0
$\vec{v}_1$	(+−−)	$S_1S_4S_6$	$\frac{V_{dc}}{2},\frac{-V_{dc}}{2},\frac{-V_{dc}}{2},\frac{-V_{dc}}{6}$	$\frac{2V_{dc}}{3},\frac{-V_{dc}}{3},\frac{-V_{dc}}{3}$
$\vec{v}_{6,1}$	(+−*)	S_1S_4	$\frac{V_{dc}}{2},\frac{-V_{dc}}{2},0,0$	$\frac{V_{dc}}{2},\frac{-V_{dc}}{2},0$
$\vec{v}_6$	(+−+)	$S_1S_4S_5$	$\frac{V_{dc}}{2},\frac{-V_{dc}}{2},\frac{V_{dc}}{2},\frac{V_{dc}}{6}$	$\frac{V_{dc}}{3},\frac{-2V_{dc}}{3},\frac{V_{dc}}{3}$
$\vec{v}_{1,2}$	(+*−)	S_1S_6	$\frac{V_{dc}}{2},0,\frac{-V_{dc}}{2},0$	$\frac{V_{dc}}{2},0,\frac{-V_{dc}}{2}$
$\vec{v}_{Z12}$	(+**)	S_1	$\frac{V_{dc}}{2},\frac{V_{dc}}{2},\frac{V_{dc}}{2},\frac{V_{dc}}{2}$	0,0,0
$\vec{v}_{Z13}$	(+*+)	S_1S_5	$\frac{V_{dc}}{2},\frac{V_{dc}}{2},\frac{V_{dc}}{2},\frac{V_{dc}}{2}$	0,0,0
$\vec{v}_2$	(++−)	$S_1S_3S_6$	$\frac{V_{dc}}{2},\frac{V_{dc}}{2},\frac{-V_{dc}}{2},\frac{V_{dc}}{6}$	$\frac{V_{dc}}{3},\frac{V_{dc}}{3},\frac{-2V_{dc}}{3}$
$\vec{v}_{Z14}$	(++*)	S_1S_3	$\frac{V_{dc}}{2},\frac{V_{dc}}{2},\frac{V_{dc}}{2},\frac{V_{dc}}{2}$	0,0,0
$\vec{v}_{Z15}$	(+++)	$S_1S_3S_5$	$\frac{V_{dc}}{2},\frac{V_{dc}}{2},\frac{V_{dc}}{2},\frac{V_{dc}}{2}$	0,0,0

2.3 3PVSI in 120°, 150°, and 180° conduction modes, QSVPWM outputs, and switching strategies

The PWM signal used in this study is the center aligned PWM with a triangular wave form as the carrier as shown in Fig. 9. The switching strategies apply the center aligned PWM to the "on" switches in Table. 1, taking into account the position of the rotor at that moment, the rotation direction of the motor, and the conduction mode selected. Tables. 2, 3, 4 summarize the switching patterns with respect to the rotor position and the direction of rotation.

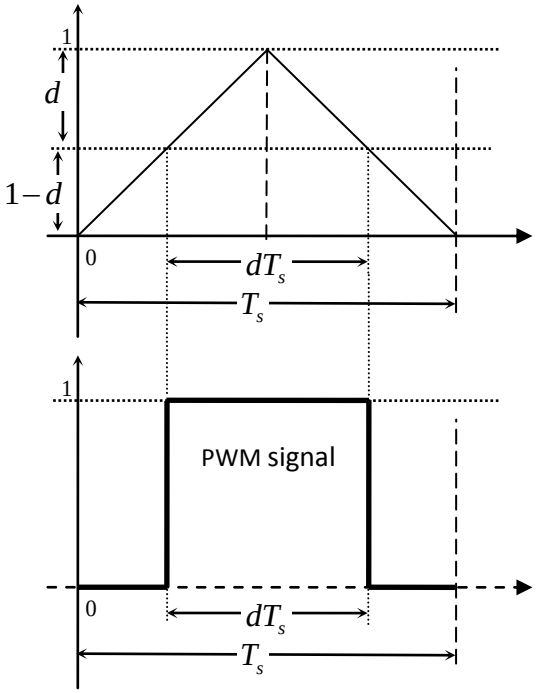

Fig.9. The center aligned PWM with d as the normalized duty cycle. The triangle carrier has a period of T_s.

The normalized duty cycle denoted d, is determined by the modified volt-second balance principle:

$$\int_0^{T_s} \left|\vec{v}_{s\_ref}\right| dt = \int_0^{dT_s} |QSV|\, dt$$

$$d = \left|\vec{v}_{s\_ref}\right| \Big/ |QSV| \qquad (9)$$

where $\left|\vec{v}_{s\_ref}\right|$ is the magnitude of the reference space vector at any sector $(1,2,\ldots,12)$ and $|QSV|$ is the magnitude of the appropriate QSV in that sector.

Table 2.120° QSVPWM switching patterns for CCW and CW rotation.

Sector no.	Range of θ_e	Switching pattern for CCW rotation	Switching pattern for CW rotation
1	$-2\pi \le \theta_e < -11\pi/6$ or $0 \le \theta_e < \pi/6$	$\vec{v}_{1,2}(+*-)$	$\vec{v}_{4,5}(-*+)$
2	$-11\pi/6 \le \theta_e < -10\pi/6$ or $\pi/6 \le \theta_e < 2\pi/6$	$\vec{v}_{1,2}(+*-)$	$\vec{v}_{4,5}(-*+)$
3	$-10\pi/6 \le \theta_e < -9\pi/6$ or $2\pi/6 \le \theta_e < 3\pi/6$	$\vec{v}_{2,3}(*+-)$	$\vec{v}_{5,6}(*-+)$
4	$-9\pi/6 \le \theta_e < -8\pi/6$ or $3\pi/6 \le \theta_e < 4\pi/6$	$\vec{v}_{2,3}(*+-)$	$\vec{v}_{5,6}(*-+)$
5	$-8\pi/6 \le \theta_e < -7\pi/6$ or $4\pi/6 \le \theta_e < 5\pi/6$	$\vec{v}_{3,4}(-+*)$	$\vec{v}_{6,1}(+-*)$
6	$-7\pi/6 \le \theta_e < -\pi$ or $5\pi/6 \le \theta_e < \pi$	$\vec{v}_{3,4}(-+*)$	$\vec{v}_{6,1}(+-*)$
7	$-\pi \le \theta_e < -5\pi/6$ or $\pi \le \theta_e < 7\pi/6$	$\vec{v}_{4,5}(-*+)$	$\vec{v}_{1,2}(+*-)$
8	$-5\pi/6 \le \theta_e < -4\pi/6$ or $7\pi/6 \le \theta_e < 8\pi/6$	$\vec{v}_{4,5}(-*+)$	$\vec{v}_{1,2}(+*-)$
9	$-4\pi/6 \le \theta_e < -3\pi/6$ or $8\pi/6 \le \theta_e < 9\pi/6$	$\vec{v}_{5,6}(*-+)$	$\vec{v}_{2,3}(*+-)$
10	$-3\pi/6 \le \theta_e < -2\pi/6$ or $9\pi/6 \le \theta_e < 10\pi/6$	$\vec{v}_{5,6}(*-+)$	$\vec{v}_{2,3}(*+-)$
11	$-2\pi/6 \le \theta_e < -\pi/6$ or $10\pi/6 \le \theta_e < 11\pi/6$	$\vec{v}_{6,1}(+-*)$	$\vec{v}_{3,4}(-+*)$
12	$-\pi/6 \le \theta_e < 0$ or $11\pi/6 \le \theta_e < 2\pi$	$\vec{v}_{6,1}(+-*)$	$\vec{v}_{3,4}(-+*)$

Table 3. 150° QSVPWM switching patterns for CCW and CW rotation.

Sector no.	Range of θ_e	Switching pattern for CCW rotation	Switching pattern for CW rotation
1	$-2\pi \le \theta_e < -11\pi/6$ or $0 \le \theta_e < \pi/6$	$\vec{v}_{1,2}(+*-)$	$\vec{v}_4(-++)$
2	$-11\pi/6 \le \theta_e < -10\pi/6$ or $\pi/6 \le \theta_e < 2\pi/6$	$\vec{v}_2(++-)$	$\vec{v}_{4,5}(-*+)$
3	$-10\pi/6 \le \theta_e < -9\pi/6$ or $2\pi/6 \le \theta_e < 3\pi/6$	$\vec{v}_{2,3}(*+-)$	$\vec{v}_5(--+)$
4	$-9\pi/6 \le \theta_e < -8\pi/6$ or $3\pi/6 \le \theta_e < 4\pi/6$	$\vec{v}_3(-+-)$	$\vec{v}_{5,6}(*-+)$
5	$-8\pi/6 \le \theta_e < -7\pi/6$ or $4\pi/6 \le \theta_e < 5\pi/6$	$\vec{v}_{3,4}(-+*)$	$\vec{v}_6(+-+)$
6	$-7\pi/6 \le \theta_e < -\pi$ or $5\pi/6 \le \theta_e < \pi$	$\vec{v}_4(-++)$	$\vec{v}_{6,1}(+-*)$
7	$-\pi \le \theta_e < -5\pi/6$ or $\pi \le \theta_e < 7\pi/6$	$\vec{v}_{4,5}(-*+)$	$\vec{v}_1(+--)$
8	$-5\pi/6 \le \theta_e < -4\pi/6$ or $7\pi/6 \le \theta_e < 8\pi/6$	$\vec{v}_5(--+)$	$\vec{v}_{1,2}(+*-)$
9	$-4\pi/6 \le \theta_e < -3\pi/6$ or $8\pi/6 \le \theta_e < 9\pi/6$	$\vec{v}_{5,6}(*-+)$	$\vec{v}_2(++-)$
10	$-3\pi/6 \le \theta_e < -2\pi/6$ or $9\pi/6 \le \theta_e < 10\pi/6$	$\vec{v}_6(+-+)$	$\vec{v}_{2,3}(*+-)$
11	$-2\pi/6 \le \theta_e < -\pi/6$ or $10\pi/6 \le \theta_e < 11\pi/6$	$\vec{v}_{6,1}(+-*)$	$\vec{v}_3(-+-)$
12	$-\pi/6 \le \theta_e < 0$ or $11\pi/6 \le \theta_e < 2\pi$	$\vec{v}_1(+--)$	$\vec{v}_{3,4}(-+*)$

Table 4. 180° QSVPWM switching patterns for CCW and CW rotation.

Sector no.	Range of θ_e	Switching pattern for CCW rotation	Switching pattern for CW rotation
1	$-2\pi \le \theta_e < -11\pi/6$ or $0 \le \theta_e < \pi/6$	$\vec{v}_1(+--)$	$\vec{v}_4(-++)$
2	$-11\pi/6 \le \theta_e < -10\pi/6$ or $\pi/6 \le \theta_e < 2\pi/6$	$\vec{v}_2(++-)$	$\vec{v}_5(--+)$
3	$-10\pi/6 \le \theta_e < -9\pi/6$ or $2\pi/6 \le \theta_e < 3\pi/6$	$\vec{v}_2(++-)$	$\vec{v}_5(--+)$
4	$-9\pi/6 \le \theta_e < -8\pi/6$ or $3\pi/6 \le \theta_e < 4\pi/6$	$\vec{v}_3(-+-)$	$\vec{v}_6(+-+)$
5	$-8\pi/6 \le \theta_e < -7\pi/6$ or $4\pi/6 \le \theta_e < 5\pi/6$	$\vec{v}_3(-+-)$	$\vec{v}_6(+-+)$
6	$-7\pi/6 \le \theta_e < -\pi$ or $5\pi/6 \le \theta_e < \pi$	$\vec{v}_4(-++)$	$\vec{v}_1(+--)$

7	$-\pi \le \theta_e < -5\pi/6$ or $\pi \le \theta_e < 7\pi/6$	$\vec{v}_4(-++)$	$\vec{v}_1(+--)$
8	$-5\pi/6 \le \theta_e < -4\pi/6$ or $7\pi/6 \le \theta_e < 8\pi/6$	$\vec{v}_5(--+)$	$\vec{v}_2(++-)$
9	$-4\pi/6 \le \theta_e < -3\pi/6$ or $8\pi/6 \le \theta_e < 9\pi/6$	$\vec{v}_5(--+)$	$\vec{v}_2(++-)$
10	$-3\pi/6 \le \theta_e < -2\pi/6$ or $9\pi/6 \le \theta_e < 10\pi/6$	$\vec{v}_6(+-+)$	$\vec{v}_3(-+-)$
11	$-2\pi/6 \le \theta_e < -\pi/6$ or $10\pi/6 \le \theta_e < 11\pi/6$	$\vec{v}_6(+-+)$	$\vec{v}_3(-+-)$
12	$-\pi/6 \le \theta_e < 0$ or $11\pi/6 \le \theta_e < 2\pi$	$\vec{v}_1(+--)$	$\vec{v}_4(-++)$

3. The dynamic modeling of 3PPMBLDC motor

Trapezoidal back EMF modeling. A 3PPMBLDC motor in this study is classified as the surface-mounted-magnet, conventional stator. It has the trapezoidal back EMF in each stator winding with the electrical angular displacement difference in each phase. The peak value of the back EMF denoted $e_m(t)$, is derived as shown in Eq. (10) [2] where K_b is the motor back EMF constant (volt/(rad/s)). We define $f_a(\theta_e)$, $f_b(\theta_e)$, and $f_c(\theta_e)$ as shown in Eq. (11) and (12). Where θ_e is the rotor electrical angular displacement. The back EMFs of the stator windings, phase a($e_a(t,\theta_e)$), phase b($e_b(t,\theta_e)$), and phase c($e_c(t,\theta_e)$) can be expressed as in Eq. (13):

$$e_m(t) = K_b \omega_m(t), \qquad (10)$$

$$f_a(\theta_e) = \begin{cases} 1 & ; -2\pi \le \theta_e \le -10\pi/6 \\ \frac{-6}{\pi}\left[\theta_e + \frac{10\pi}{6}\right] + 1 & ; -10\pi/6 \le \theta_e \le -8\pi/6 \\ -1 & ; -8\pi/6 \le \theta_e \le -4\pi/6 \\ \frac{6}{\pi}\left[\theta_e + \frac{4\pi}{6}\right] - 1 & ; -4\pi/6 \le \theta_e \le -2\pi/6 \\ 1 & ; -2\pi/6 \le \theta_e \le 2\pi/6 \\ \frac{-6}{\pi}\left[\theta_e - \frac{2\pi}{6}\right] + 1 & ; 2\pi/6 \le \theta_e \le 4\pi/6 \\ -1 & ; 4\pi/6 \le \theta_e \le 8\pi/6 \\ \frac{6}{\pi}\left[\theta_e - \frac{8\pi}{6}\right] - 1 & ; 8\pi/6 \le \theta_e \le 10\pi/6 \\ 1 & ; 10\pi/6 \le \theta_e \le 2\pi \end{cases} \qquad (11)$$

$$f_b(\theta_e) = f_a(\theta_e - \frac{2\pi}{3}),\ f_c(\theta_e) = f_a(\theta_e + \frac{2\pi}{3}) \qquad (12)$$

,

$$\begin{aligned} e_a(t,\theta_e) &= f_a(\theta_e) e_m(t), \\ e_b(t,\theta_e) &= f_b(\theta_e) e_m(t) \text{ and} \\ e_c(t,\theta_e) &= f_c(\theta_e) e_m(t). \end{aligned} \qquad (13)$$

The electromagnetic torque, rotational equation of motion, the rotor mechanical and electrical angular velocities and displacements.

The electromagnetic torque denoted T_e can be expressed as shown in Eq. (14) where $\omega_m(t)$ is the mechanical angular velocity of the rotor :

$$\begin{aligned} T_e(t,\theta_e) &= \frac{e_a(t,\theta_e) i_a + e_b(t,\theta_e) i_b + e_c(t,\theta_e) i_c}{\omega_m(t)}. \\ &= K_b [\, f_a(\theta_e) i_a + f_b(\theta_e) i_b + f_c(\theta_e) i_c \,] \end{aligned} \qquad (14)$$

The rotational equation of motion. The rotational equation of motion can be expressed as in Eq. (15) where J_m is the moment of inertia of the rotor including mechanical loads attached. B_m is the viscous damping between the rotor and the environment contacted. T_l is the load torque

disturbed through the axle of rotor Eq. (15) is as follows:

$$J_m \frac{d\omega_m}{dt} + B_m \omega_m = T_e - T_l \,. \qquad (15)$$

The rotor mechanical and electrical angular velocities and displacements. The rotor electrical angular velocity denoted $\omega_e(t)$, is defined as in Eq. (16) where p is the number of poles of permanent magnets attached to the rotor :

$$\omega_e(t) = \frac{d\theta_e}{dt} = \left(\frac{p}{2}\right)\frac{d\theta_m}{dt} = \frac{p}{2}\omega_m(t) \,. \qquad (16)$$

The state space equation of 3PPMBLDC motor. Under the assumptions of $i_a + i_b + i_c = 0$, the mutual inductance between each phase winding is equal to the others and is defined as M. The self inductance of each phase winding is equal to the others and defined as L. The resistance of each phase winding is equal to the others and defined as R_p. We define $L_p = L - M$, the state space equation of 3PPMBLDC motor which can be written as in Eq. (17).

$$\begin{bmatrix} \frac{di_a}{dt} \\ \frac{di_b}{dt} \\ \frac{di_c}{dt} \\ \frac{d\theta_m}{dt} \\ \frac{d\omega_m}{dt} \end{bmatrix} = \begin{bmatrix} \frac{-R_p}{L_p} & 0 & 0 & 0 & \frac{-f_a(\theta_e)K_b}{L_p} \\ 0 & \frac{-R_p}{L_p} & 0 & 0 & \frac{-f_b(\theta_e)K_b}{L_p} \\ 0 & 0 & \frac{-R_p}{L_p} & 0 & \frac{-f_c(\theta_e)K_b}{L_p} \\ 0 & 0 & 0 & 0 & 1 \\ 0 & 0 & 0 & 0 & \frac{-B_m}{T_m} \end{bmatrix} \begin{bmatrix} i_a \\ i_b \\ i_c \\ \theta_m \\ \omega_m \end{bmatrix}$$

$$+ \begin{bmatrix} \frac{1}{L_p} & 0 & 0 & 0 & 0 \\ 0 & \frac{1}{L_p} & 0 & 0 & 0 \\ 0 & 0 & \frac{1}{L_p} & 0 & 0 \\ 0 & 0 & 0 & 0 & 0 \\ 0 & 0 & 0 & \frac{1}{J_m} & \frac{-1}{J_m} \end{bmatrix} \begin{bmatrix} V_{an} \\ V_{bn} \\ V_{cn} \\ T_e \\ T_l \end{bmatrix} \qquad (17)$$

4. Simulation Results and Discussion

The torque, speed, current and back EMF characteristics of 3PPMBLDC motor when driven by 3PVSI in the 120°, 150° and 180° QSPWM are investigated with the following motor parameters: $V_{dc} = 36$ volt, $R_p = 0.5\Omega$, $L_p = 0.005H$, $p = 46$ poles, $J_m = 2\ kgm^2$, $B_m = 0.2\ N-m/(rad/s)$, and $K_b = 2.45\ volt/(rad/s)$. The sampling frequency for PWM generation during the simulation is $1\,kHz$. The simulation duration is 5 seconds. The spectral plots of ω_m, and T_e are considered during the period in which the 3PPMBLDC motor is in the steady state (as observed from the time- domain simulated plots) of which the start time is from the 3rd second to the end of simulation. The fundamental frequency is set to 1 Hz with 2 cycles to cover the signals of interest until the end of the simulation. The maximum frequency of the spectrum is 500 Hz.

Table 5. Parameters for simulations.

Parameters	Value	Units
DC link power supply	36	Volt
Phase winding resistance (R_p)	0.5	Ohm

Self against Mutual inductance difference (L_p)	0.005	Henry
No. of rotor poles (p)	46	pole
Rotor moment of inertia (J_m)	2.0	$kg-m^2$
Viscous damping (B_m)	0.2	$\frac{N-m}{rad/s}$
Back emf constant (K_b)	2.45	$\frac{volt}{rad/s}$
Sampling frequency $(f_{carrier})$	1000	Hz

From Fig. 10, 16, and 22, it can be seen that with the same 100% duty cycle, driving 3PPMBLDC motor with 150° conduction mode yields the highest steady state ω_m of 11.52 rad/s. This is because each QSV in the 150° conduction mode stays closer to the next one by an amount of $\pi/6$ rad that produces the rotating magnetomotive force which is aligned much closer to the right angle to the rotor magnetomotive force, resulting in a better tangential torque acting upon the rotor.

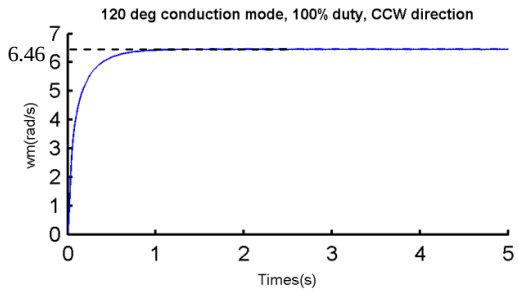

Fig.10. ω_m plot when we use a 3PVSI in the 120° conduction mode and 100% duty cycle in CCW direction.

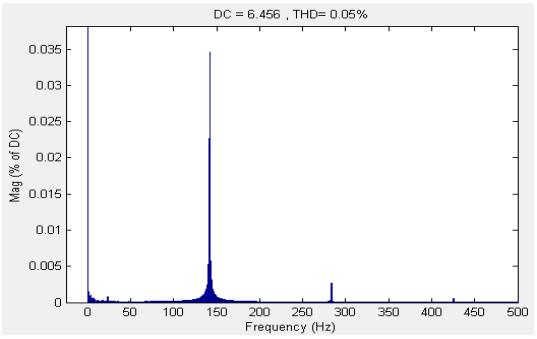

Fig.11. Spectral plot of ω_m when we use a 3PVSI in the 120° conduction mode and 100% duty cycle in CCW direction.

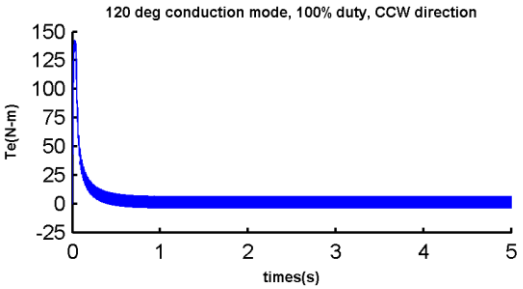

Fig.12. T_e plot when we use a 3PVSI in the 120° conduction mode and 100% duty cycle in CCW direction.

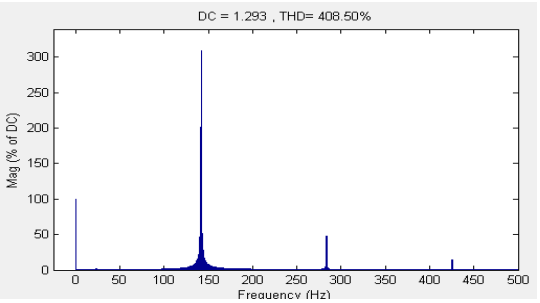

Fig.13. Spectral plot of T_e when we use a 3PVSI in the 120° conduction mode and 100% duty cycle in CCW direction.

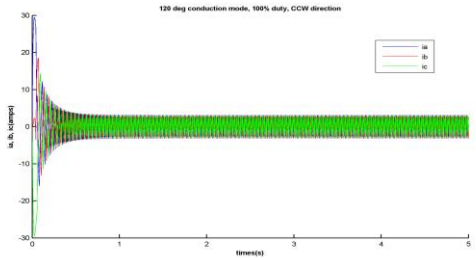

Fig.14. i_a, i_b, i_c plot when we use a 3PVSI in the 120° conduction mode and 100% duty cycle in CCW direction.

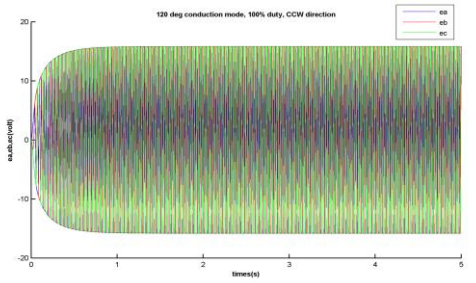

Fig.15. e_a, e_b, e_c plot when we use a 3PVSI in the 120° conduction mode and 100% duty cycle in CCW direction.

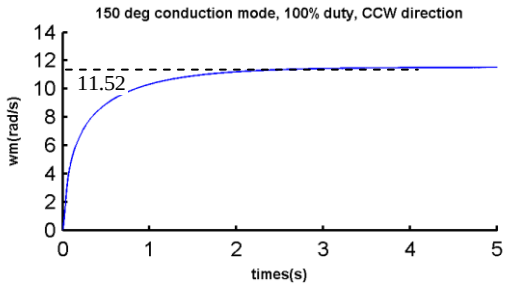

Fig.16. ω_m plot when we use a 3PVSI in the 150° conduction mode and 100% duty cycle in CCW direction.

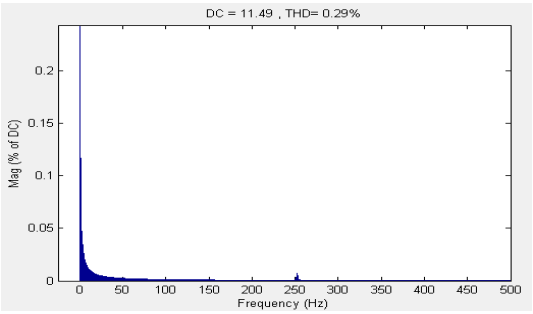

Fig.17. Spectral plot of ω_m when we use a 3PVSI in the 150° conduction mode and 100% duty cycle in CCW direction.

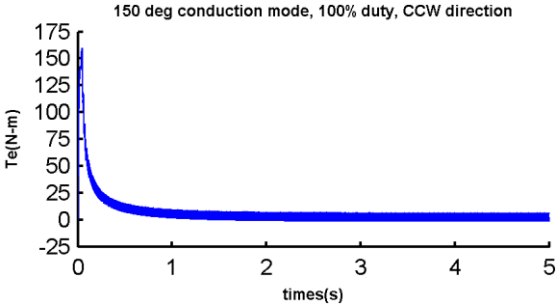

Fig.18. T_e plot when we use a 3PVSI in the 150° conduction mode and 100% duty cycle in CCW direction.

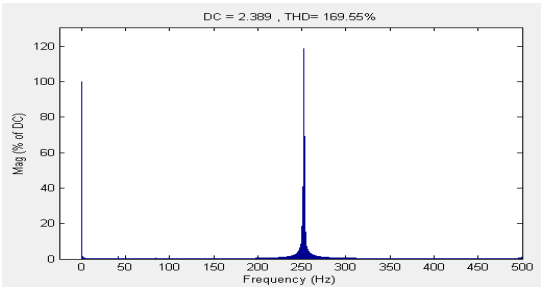

Fig.19. Spectral plot of T_e when we use a 3PVSI in the 150° conduction mode and 100% duty cycle in CCW direction.

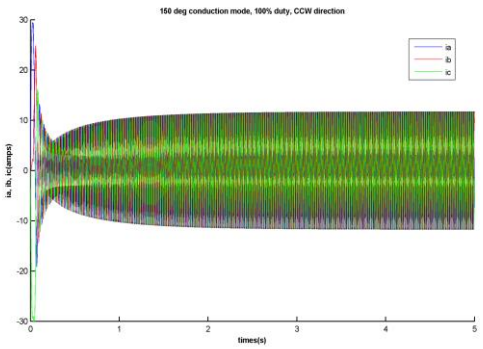

Fig.20. i_a, i_b, i_c plot when we use a 3PVSI in the 150° conduction mode and 100% duty cycle in CCW direction.

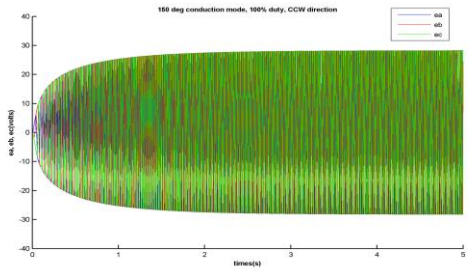

Fig.21. e_a, e_b, e_c plot when we use a 3PVSI in the 150° conduction mode and 100% duty cycle in CCW direction.

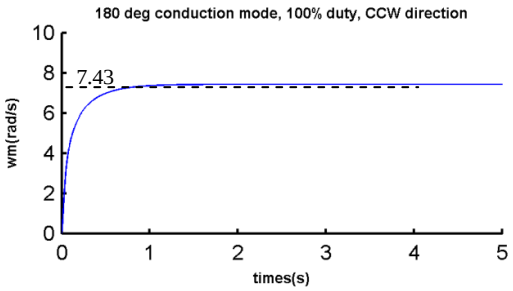

Fig.22. ω_m plot when we use a 3PVSI in the 180° conduction mode and 100% duty cycle in CCW direction.

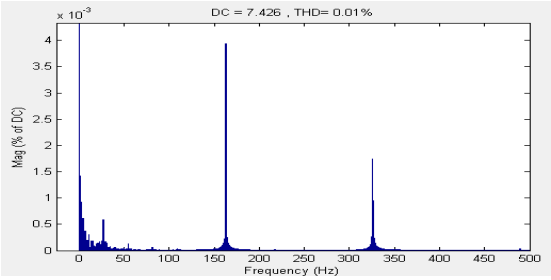

Fig.23. Spectral plot of ω_m when we use a 3PVSI in the 180° conduction mode and 100% duty cycle in CCW direction

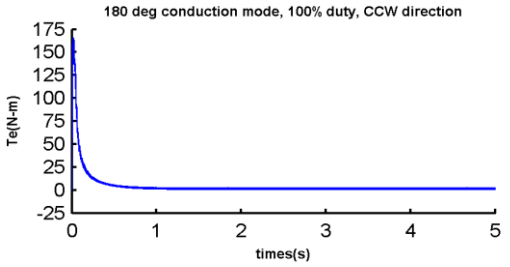

Fig.24. T_e plot when we use a 3PVSI in the 180° conduction mode and 100% duty cycle in CCW direction.

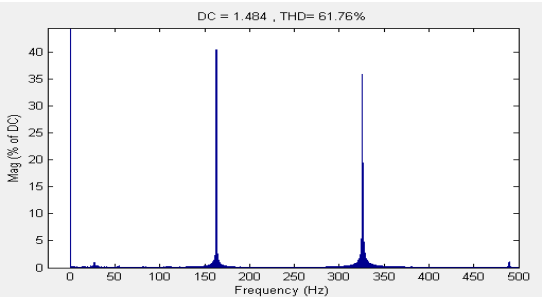

Fig.25. Spectral plot of T_e when we use a 3PVSI in the 180° conduction mode and 100% duty cycle in CCW direction.

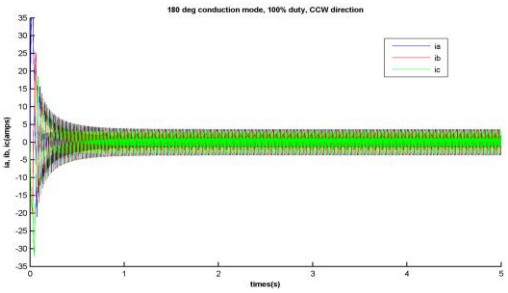

Fig.26. i_a, i_b, i_c plot when we use a 3PVSI in the 180° conduction mode and 100% duty cycle in CCW direction.

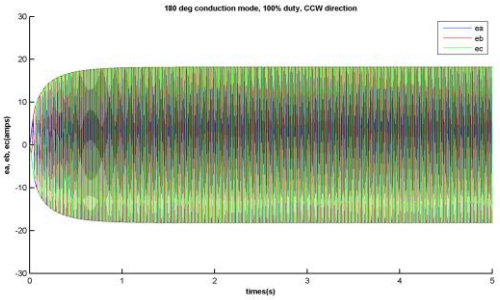

Fig.27. e_a, e_b, e_c plot when we use a 3PVSI in the 180° conduction mode and 100% duty cycle in CCW direction.

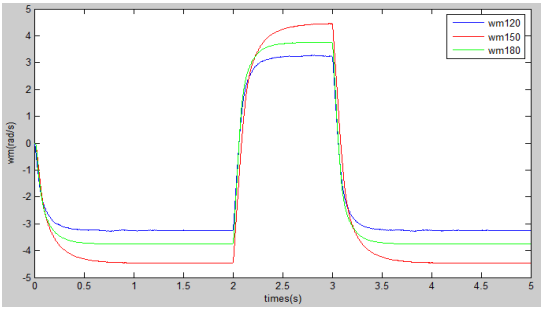

Fig.28. ω_m plots when we use a 3PVSI in the 120°, 150°, 180° conduction mode and 50% duty cycle in both CW and CCW directions.

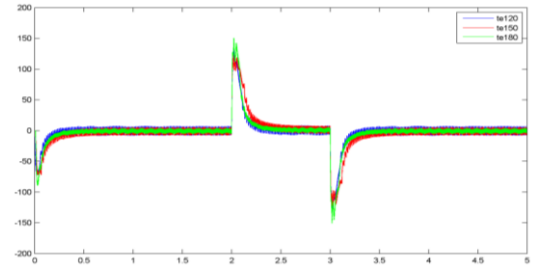

Fig.29. T_e plots when we use a 3PVSI in the 120°, 150°, 180° conduction mode and 50% duty cycle in both CW and CCW directions.

On the other hand, the 150° conduction mode QSPWM produces a slightly higher %THD of ω_m. This is because there are more step transitions (12 QSVs for the 150° conduction mode QSPWM) in a rotation cycle. From Fig. 12, 18, 24, the maximum T_e that can be achieved for the 150° and for the 180° conduction mode QSPWMs is almost the same and higher than in the 120° conduction mode QSPWM. In addition, the 180° conduction mode QSPWM produces the lowest %THD of T_e whereas the 120° conduction mode QSPWM produces the highest %THD of T_e because each stator phase winding in the 120° conduction mode QSPWM is idle for at least $2\pi/3$ in each switching cycle as can be seen in Fig. 3 when $V_{an}=0$, causing an abrupt increase in the value of T_e while each stator winding in the 180° conduction mode QSPWM is always energized, thus avoiding sudden changes in the value of T_e.

5. Conclusions

This paper proposes three modulation schemes for a conventional 3PVSI that require less computation and are suitably acceptable for low precision applications such as electric bike motor drive and quad rotor robot motor drive. They are based on the QSVs. The appropriate QSV closest to the right angle to the rotor position is selected as the switching pattern to follow as in Tables 2, 3, 4 depending on the conduction mode selected. It is clear from the simulation results that driving 3PPMBLDC motor by 3PVSI with the 150° conduction mode QSPWM yields the highest ω_m with a compromisable %THD. In addition, the maximum T_e produced by this conduction mode QSPWM is almost the highest. Therefore, in terms of ω_m, T_e and %THDs, it is promising to choose the 150° conduction mode QSPWM as an alternative modulation scheme for 3PVSI driving 3PPMBLDC motor.

6. References

[1] Atif Iqbal, Shaikh Moinuddin, Assessment of Torque Pulsation in Inverter Fed Three-Phase Induction Motor Drive for 180° and 150° Conduction Modes, International Conference on Information and Communication Technology in Electrical Sciences(ICTES 2007), Tamil Nadu India, pp.323-328, 2007.

[2] P. Tripura, Y.S. Kishore Babu, and Y. R. Tagore, Space Vector Pulse Width Modulation Schemes for Two-Level Voltage Source Inverter, ACEEE Int.J. on Control System and Instrumentation, vol. 02, no. 3 (2011) 34-38.

[3] Devisree Sasi, and Jisha Kuruvilla P, Modelling and Simulation of SVPWM Inverter Fed Permanent Magnet Brushless DC Motor Drive, ACEEE Int.J. of Advanced Research in Electrical, Electronics, and Instrumentation Engineering, vol. 02, issue. 5 (2013) 1947-1955.

[4] Mahmoud M. Gaballah, Design and Implementation of Space Vector PWM Inverter Based on a Low Cost Microcontroller, Arab J Sci Eng, no. 38 (2013) 3059–3070.

[5] G. Prasad, N. Sree Ramya, P.V.N. Prasad, and G. Tulasi Ram Das, Modelling and Simulation Analysis of the Brushless DC motor by using MATLAB, IJITEE Int.J. of Innovative Technology and Exploring Engineering, vol. 01, issue. 5 (2012) 27-31.

[6] Yong Liu, Z. Q. Zhu, and David Howe, Direct Torque Control of Brushless DC Drives With Reduced Torque Ripple, IEEE Trans. on Industry Applications, vol. 41, no. 2, March/April (2005) 599-608.

[7] Jawad Faiz, M. R. Azizian, and M. Aboulghasemian-Azami, Simulation and Analysis of Brushless DC Motor Drives using Hysteresis, Ramp Comparison and Predictive Current Control Techniques, Elsevier Int.J. of Simulation Practice and Theory, vol. 03,(1996) 347-363.

[8] Bimal K Bose, Modern Power Electronics and AC Drives, Pearson Education Publications, New Delhi, 2002.

[9] R Krishnan, Electric Motor Drives: Modeling, Analysis, and Control, Prentice Hall, Inc, 2001.

[10] Ming-Fa Tsai,Tran Phu Quy, Bo-Feng Wu, and Chung-Shi Tseng, Model Construction and Verification of a BLDC Motor Using MATLAB/SIMULINK and FPGA Control, IEEE conference on Industrial Electronics and Applications (ICIEA), 6th (2011) 1797-1802.